Role of tropospheric ozone increases in 20th-century climate change

Drew Shindell,[1,2] Greg Faluvegi,[1,2] Andrew Lacis,[1,3] James Hansen,[1,2] Reto Ruedy,[4] and Elliot Aguilar[1,2]

Received 9 June 2005; revised 14 December 2005; accepted 20 January 2006; published 28 April 2006.

[1] Human activities have increased tropospheric ozone, contributing to 20th-century warming. Using the spatial and temporal distribution of precursor emissions, we simulated tropospheric ozone from 1890 to 1990 using the NASA Goddard Institute for Space Studies (GISS) chemistry model. Archived three-dimensional ozone fields were then used in transient GISS climate model simulations. This enables more realistic evaluation of the impact of tropospheric ozone increases than prior simulations using an interpolation between preindustrial and present-day ozone. We find that tropospheric ozone contributed to the greater 20th-century warming in the Northern Hemisphere extratropics compared with the tropics and in the tropics compared with the Southern Hemisphere extratropics. Additionally, ozone increased more rapidly during the latter half of the century than the former, causing more rapid warming during that time. This is especially apparent in the tropics and is consistent with observations, which do not show similar behavior in the extratropics. Other climate forcings do not substantially accelerate warming rates in the tropics relative to other regions. This suggests that accelerated tropospheric ozone increases related to industrialization in the developing world have contributed to the accelerated tropical warming. During boreal summer, tropospheric ozone causes enhanced warming (>0.5°C) over polluted northern continental regions. Finally, the Arctic climate response to tropospheric ozone increases is large during fall, winter, and spring when ozone's lifetime is comparatively long and pollution transported from midlatitudes is abundant. The model indicates that tropospheric ozone could have contributed about 0.3°C annual average and about 0.4°C–0.5°C during winter and spring to the 20th-century Arctic warming. Pollution controls could thus substantially reduce the rapid rate of Arctic warming.

Citation: Shindell, D., G. Faluvegi, A. Lacis, J. Hansen, R. Ruedy, and E. Aguilar (2006), Role of tropospheric ozone increases in 20th-century climate change, *J. Geophys. Res.*, *111*, D08302, doi:10.1029/2005JD006348.

1. Introduction

[2] Ozone in the lower atmosphere is thought to have increased substantially since preindustrial times. Tropospheric ozone is both a surface level pollutant, causing respiratory problems in humans and reducing agricultural yields, and a greenhouse gas leading to global warming. Current estimates assign a global annual average adjusted tropopause radiative forcing value of 0.35 ± 0.15 W m^{-2} to tropospheric ozone increases since the preindustrial on the basis of simulations with chemical models [*Ramaswamy et al.*, 2001]. While many models have simulated the total preindustrial-to-present tropospheric ozone change by simply removing all anthropogenic emissions [*Berntsen et al.*, 1997; *Hauglustaine and Brasseur*, 2001; *Levy et al.*, 1997; *Mickley et al.*, 1999; *Roelofs et al.*, 1997; *Shindell et al.*, 2003; *Wang and Jacob*, 1998], the change as a function of time has received much less attention [*Berntsen et al.*, 2000; *Stevenson et al.*, 1998]. Thus transient climate simulations to date have used linear interpolation between preindustrial and present-day values [*Roeckner et al.*, 1999], exponential interpolation [*Hansen et al.*, 2002] or scaling by carbon dioxide emissions [*Dai et al.*, 2001; *Kiehl et al.*, 1999; *Meehl et al.*, 2004]. Given the nonlinear pace of economic development, and its variation in different parts of the world, the true changes in ozone as a function of time and space are likely to be considerably more complex, however. Recently, historical emissions data sets have been created [*van Aardenne et al.*, 2001], allowing simulations of tropospheric ozone as a function of time and space. This should facilitate improved estimates of the contribution of tropospheric ozone changes to recent climate trends.

[3] Unlike the well-mixed greenhouse gases, ozone is short lived relative to transport times within the troposphere,

[1]NASA Goddard Institute for Space Studies, New York, New York, USA.
[2]Earth Institute, Columbia University, New York, New York, USA.
[3]Department of Earth and Environmental Sciences, Columbia University, New York, New York, USA.
[4]SGT Incorporated, New York, New York, USA.

Copyright 2006 by the American Geophysical Union.
0148-0227/06/2005JD006348

and is therefore distributed inhomogeneously. A large fraction of the emissions of ozone precursors are from human activities, and anthropogenic emissions dominate the preindustrial to present-day tropospheric ozone change. The largest changes would be expected to have occurred relatively close to the location of precursor emission increases, thus primarily in the Northern Hemisphere (NH) and largely over land areas. However, the radiative forcing per unit ozone change maximizes near the tropopause [*Hansen et al.*, 1997], far enough from the surface emissions that ozone and many of its precursors are more evenly distributed and more strongly influenced by latitudinal variations in photochemical reaction rates, which are generally faster closer to the equator. Thus the radiative forcing from ozone, and especially its variation with time, results from a complex interplay between emissions, chemistry and transport. Hence evaluation of the effects of this forcing requires three-dimensional models including all these processes. Here we use a suite of models developed at the NASA Goddard Institute for Space Studies (GISS) to evaluate the time-dependent change in tropospheric ozone abundance and the climate response to this forcing.

2. Experimental Setup

[4] Tropospheric ozone changes were calculated using the GISS model II' chemistry-climate model [*Shindell et al.*, 2003]. The chemistry includes HO_x-NO_x-O_x-CO-CH_4, hydrocarbon families and peroxyacetylnitrates, and a fairly detailed treatment of organic nitrate and organic peroxide reactions. It contains complete sources and sinks for its 32 gases. The model was run at 4 by 5 degree horizontal resolution with 23 vertical layers, and the chemistry was fully coupled with the climate model's hydrological cycle and meteorology. As documented previously [*Shindell et al.*, 2003], that model version gave a fairly good simulation of troposphere ozone for the present day, though there were some discrepancies associated with stratospheric influx at high latitudes. These have a fairly small effect on radiative forcing, however, and minimal influence on the trends reported on here as they do not change with time. The adjusted global annual average radiative forcing due to preindustrial to present-day tropospheric ozone change in that model, 0.30–0.33 W m^{-2} depending on emissions, is in good agreement with the 0.35 ± 0.15 W m^{-2} range of values seen in other chemical models [*Ramaswamy et al.*, 2001]. In this model chemistry calculations were performed up to 150 hPa. Above this level, stratospheric ozone and NO_x are fixed at present-day values in all the runs. Similar preindustrial-to-present-day chemistry simulations have been recently performed within the newer GISS modelE general circulation model (GCM) using a tropopause following upper boundary, which adds to the tropospheric chemistry domain in the tropical upper troposphere (the historical simulations were performed with the older model while development of the new model took place). For emission changes identical to those that gave a forcing of 0.30 W m^{-2} in this model, those runs yielded a forcing of 0.37 W m^{-2} [*Shindell et al.*, 2005a], suggesting that the model II' results may underestimate changes by ~20% because of exclusion of the tropical upper troposphere.

[5] The chemistry model was driven by changes in the imposed emissions. Geographic distributions of emissions of the ozone precursor NO_x, CO, and nonmethane volatile organic compounds (NMVOCs) were prescribed according to *van Aardenne et al.* [2001]. This inventory of historical emissions includes sources that are entirely anthropogenic such as fossil fuel combustion and production, biofuel combustion, and industrial processes. It also includes biomass burning, with contributions from savannah burning, deforestation, and agricultural waste burning. While the latter two components are entirely anthropogenic, savannah burning includes both natural and human contributions in this inventory. Natural wildfires outside savannah regions are not accounted for, and while their contribution is relatively small in most regions, they may lead to substantial emissions in boreal areas. Emissions of NO_x from soils also contain both natural and anthropogenic contributions, with the application of fertilizers assumed to have roughly doubled the preindustrial emissions. Changes in NMVOCs are not speciated in the inventory, so all anthropogenic NMVOC species in our model were changed by the same percentage (natural NMVOCs were not changed in the simulations). Methane's abundance, imposing the present-day percentage interhemispheric gradient, was prescribed according to observations. Equilibrium simulations were performed for 1890, 1910, 1930, 1950, 1960, 1970, 1980, and 1990, with increased temporal frequency in the latter half of the 20th century since emissions changes were more rapid during those decades. Figure 1 shows the global annual average surface emissions of ozone precursors and the abundance of methane. A sample of regionally averaged surface emissions is also shown for NO_x. Emissions of NO_x from aircraft were prescribed using our 1992 GEIA inventory [*Baughcum et al.*, 1996] and scaling in the past following US trends [*United States Environmental Protection Agency*, 2000], which should be reasonably representative of global aircraft usage. This resulted in emissions of 0.008, 0.015, 0.273, 0.403, and 0.600 Tg N/yr for the decades of 1950 through 1990, and no emissions prior to 1950. Aside from varying trace gas emissions and the abundance of methane, all other conditions were unchanged. As shown in previous work [*Grenfell et al.*, 2001], the influence of climate change between the preindustrial and the present has been very small in comparison with emissions changes. We thus neglect those changes to create a simpler set of simulations that can be interpreted as the ozone response to precursor emissions and methane abundance changes alone. Thus climate-sensitive lightning NO_x emissions, which are calculated internally by the GCM and biogenic isoprene emissions did not vary in this study.

[6] The model was run for 10 years for each set of emissions. We report here on average results for the last 8 years of the runs. Given that methane values were prescribed, the 2 year spin-up should be adequate to allow full equilibration with the emissions since all other chemical timescales are much shorter and interhemispheric exchange times, the longest transport timescale in the troposphere, are

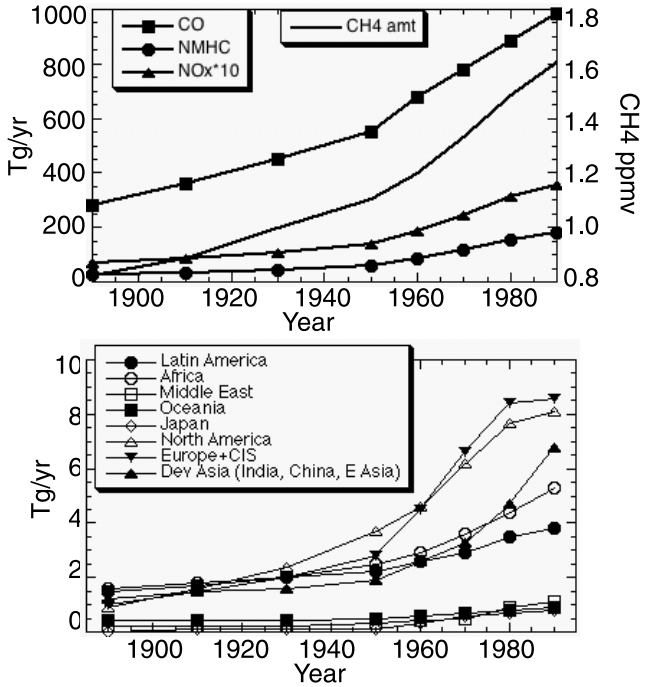

Figure 1. (top) Surface emissions of ozone precursors and methane abundances versus time. Global annual average precursor emissions (left axis) and prescribed methane abundances (right axis) are shown. (bottom) Regional annual average NO_x emissions, an example of those used for the various precursors. Emissions are based on work by *van Aardenne et al.* [2001] in Tg yr^{-1}: N for NO_x, CO for carbon monoxide, and C for nonmethane hydrocarbons. Methane was prescribed at the surface with the global mean amount shown above and a variation with latitude similar to present-day observations, creating an interhemispheric gradient of 5.5% more in the NH than the SH mean values. In the legend, CIS is the Commonwealth of Independent States (former Soviet Union), and Dev is developing. Symbols are given for years when simulations were performed.

about 1 to 2 years. The 8-year averages are long enough to smooth out interannual variability as well.

3. Ozone Changes

[7] It is impractical to present a complete view of the full set of four dimensional ozone fields that were created from the model. As simple metrics, we show global annual average values of the tropospheric ozone burden and the tropospheric ozone column (Figure 2, top). The burden is calculated as all ozone below 150 hPa, so includes some stratospheric ozone. Since ozone in the stratosphere is constant in these simulations, changes reflect tropospheric ozone only. The tropospheric ozone column is calculated as all ozone from the surface up to either a limit of 150 ppbv ozone or 150 hPa height, whichever is reached first. It is immediately clear that the two quantities show a very similar nonlinear rate of increase, though the trends in the burden are smoother. The impact of ozone on climate is more closely related to its radiative forcing, which is shown in Figure 2 (bottom). This instantaneous forcing was calculated by the GISS GCM's radiation code in response to the imposition of the model-derived ozone changes. The forcing shows a similar time dependence to the global column. It exhibits a strong spatial dependence as well, with the northern extratropical forcing increasing faster than the global or tropical averages, while the southern extratropical forcing increases more slowly. The total instantaneous forcing from 1880 to 1990 is 0.41 W m^{-2}, while the adjusted forcing (allowing stratospheric temperature to respond to the forcing) over the same time period is 0.34 W m^{-2}. This value is slightly larger than the 0.30 W m^{-2} reported for our earlier preindustrial-to-present-day simulations. The difference results from altering the definition of the tropopause, which followed fixed pressure surfaces in the earlier work and now uses the meteorological tropopause, which we believe is a more appropriate definition. The adjusted forcing is more indicative of the climate impacts of tropospheric ozone changes [*Hansen et al.*, 1997], however the time dependence of the instantaneous forcing is representative of both quantities.

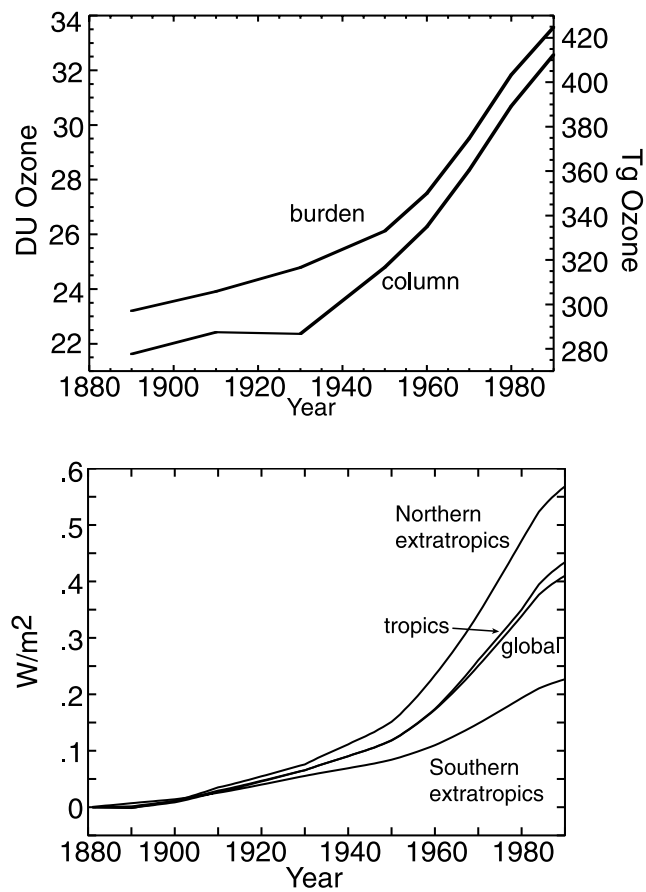

Figure 2. (top) Tropospheric ozone change calculated in the chemistry-climate model and (bottom) the resulting instantaneous tropopause radiative forcing used in the transient climate simulations, which are driven by imposed tropospheric ozone trends. Ozone changes are given both as global mean tropospheric column (>150 ppbv ozone) and tropospheric burden (below 150 hPa).

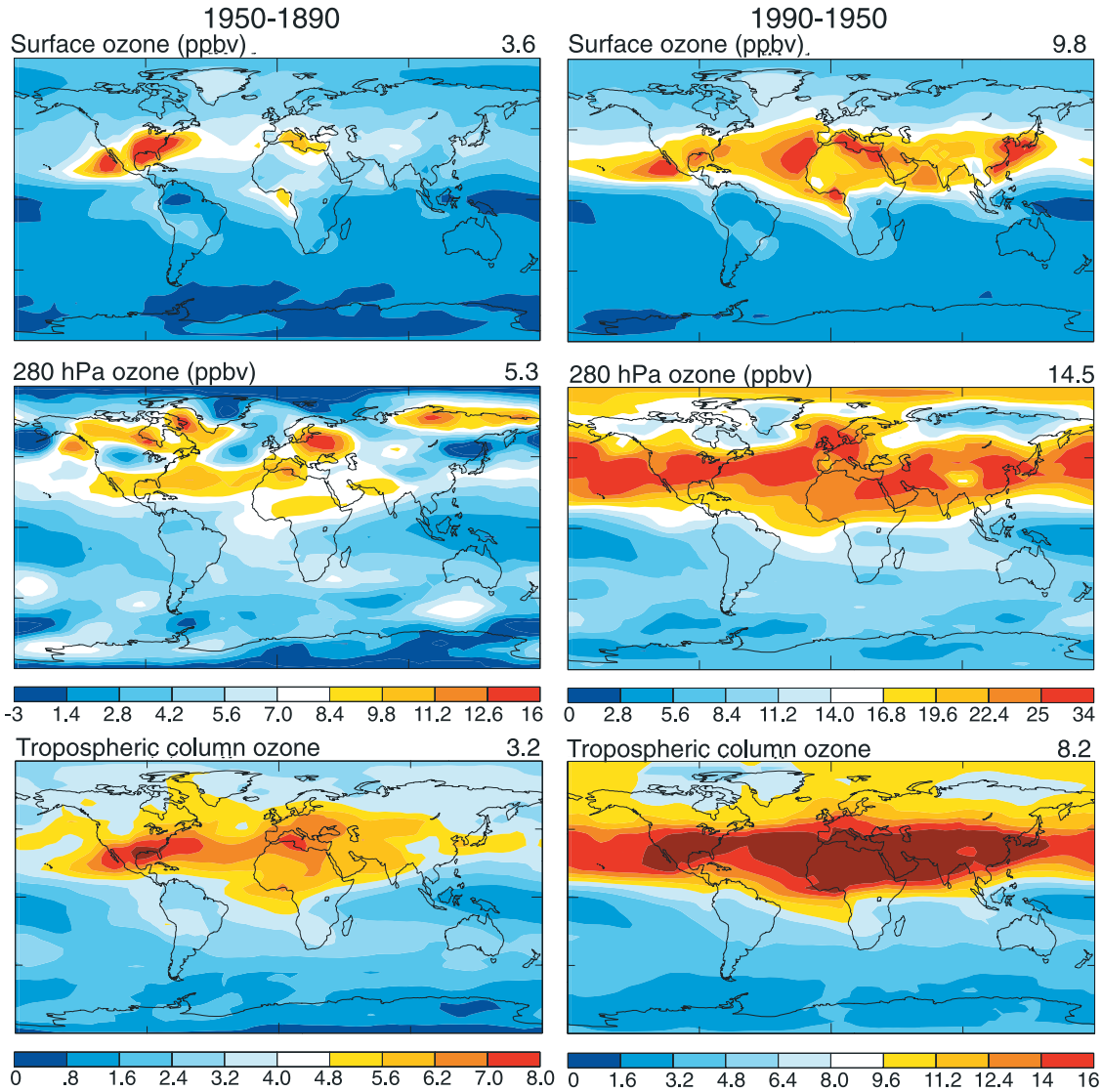

Figure 3. Ozone changes before and after 1950. Values are presented for (top) the surface level (ppbv), (middle) the level centered around 280 hPa (ppbv), and (bottom) the tropospheric column (DU). Note that the top two rows share the same color bar and that the scales in the plots on the right are twice those on the left. Values at the top right corner of each plot give the global average value in the same units as the plots.

[8] While the radiative forcing trends were nonlinear in time, they separate into two nearly linear periods: before and after 1950. Thus we focus much of our analysis on trends during the first and second halves of the 20th century. The spatial pattern of ozone changes during these two 50-year periods is shown for the surface, a level near the tropopause, and for the total column in Figure 3. The surface shows the most inhomogeneous distribution, with ozone increases clearly localized near industrialized (and to a lesser extent biomass burning) regions, especially during the first half of the century. Increases are more evenly distributed in the zonal direction at higher levels, as would be expected from the prevailing circulation and longer chemical timescales at these altitudes. Both surface and tropopause level ozone, as well as the column, show the largest increases at northern middle latitudes. Over Africa, however, the increases are nearly as large all the way to the equator. Over the oceans, the increases have been large over the Atlantic and especially over the Indian Ocean, but somewhat smaller over the Pacific.

[9] Little historical ozone data is available against which to evaluate the model simulations. Nineteenth century paper-based Schönbein measurements are unfortunately not quantitatively reliable [*Pavelin et al.*, 1999]. The oldest reliable data covering several sites with multiple measurements are surface observations from rural locations in the Alps, southern Germany and France taken during the 1930s [*Staehelin et al.*, 1994]. Averaging together all these 1930s observations yields a surface ozone value of approximately 25 ppbv. Averaging together the five grid boxes covering the central European area of observations, the model has 23 ppbv surface level ozone for 1930 conditions. The

observations were taken at stations ranging from 400 to 3450 m above sea level in altitude, with the highest mountaintop sites sampling higher air than the surface level of the model as the GCM's topography is averaged over relatively large grid boxes. We also calculated the model's average ozone value in the second layer, which was 28 ppbv for 1930. It thus appears that the model does a good job of capturing the early European surface ozone values. Extensive present-day comparisons shown previously [*Shindell et al.*, 2003] also indicated a high-quality simulation, leading us to conclude that on the basis of the limited data available, the modeled historical ozone trends are quite plausible. We note, however, that the early ozone measurements extend from the late 1930s through the 1950s. If we instead use the modeled 1950 surface values, the model trends back from the present are too small to match those observations. Similarly, if we compare the late 19th-century Montsouris observations [*Volz and Kley*, 1988] with the model, the model's surface ozone is too large (by ~10–15 ppbv). To match this measurement, the modeled trend would have to be increased by ~50%. Given that there is only a single quantitatively reliable 19th-century observation, and that even that requires an uncertain correction for aerosol contamination and may not be representative since it was taken just outside Paris, the amount of ozone in the nineteenth century is poorly constrained by observations.

[10] Likewise, modeling studies depend upon emissions that are also not well known. A prime example is emissions from biomass burning. These are partly anthropogenic and partly natural. However, even the natural component has been affected by wildfire management practices. Preindustrial biomass burning emissions are not well known, and even estimates of present-day emissions vary considerably. The data set used here [*van Aardenne et al.*, 2001] has 290 Tg CO yr^{-1} in 1990 from biomass burning, for example, while the 1990 Global Emissions Inventory Activity (GEIA) [*Benkovitz et al.*, 1996] and 2000 Global Fire Emissions Database (GFED) [*Van der Werf et al.*, 2003] inventories have 490 and 467 Tg CO yr^{-1}, respectively. In a previous study comparing modeled CO with observations from the MOPITT satellite instrument [*Shindell et al.*, 2005b], we found the best agreement using the larger inventories. Assuming the same time dependence (in percentage) as in the [*van Aardenne et al.*, 2001] data set but this larger present-day emission would roughly double the emissions increase during the 20th century from biomass burning. There is therefore considerable uncertainty as to the overall preindustrial-to-present-day tropospheric ozone change. On the basis of the comparison with the sparse early data, and the low-end biomass burning emissions, it seems possible that our results could reflect a lower bound on the tropospheric trends. This is in accord with other studies suggesting that the total change could have been larger by around a factor of two compared with values obtained from modeling studies relying upon conventional emissions estimates, on the basis of modeling work [*Mickley et al.*, 2001] and analysis of multiple early data sets [*Shindell and Faluvegi*, 2002].

[11] We can also compare with two other modeling studies investigating tropospheric ozone changes over the same time period. One study used the same set of time-dependent anthropogenic emissions of ozone precursors to drive chemical simulations with the MOZART-2 model [*Lamarque et al.*, 2005], while the other used a similar, but separately derived, set of emissions within the OsloCTM-1 [*Berntsen et al.*, 2000]. The tropospheric ozone burdens in both models increase fairly slowly from 1890 through 1950, after which the growth rate increases markedly, resulting in nearly linear trends over the two half century periods in good agreement with our tropospheric ozone results (Figure 2).

[12] The surface ozone responses in the GISS and MOZART-2 models are also quite similar. Both show the largest increases during the first half of the 20th century taking place in the Northern Hemisphere with similar spatial patterns having maxima over western Europe, near California, and especially over the eastern United States. Maximum increases in surface ozone are around 15 ppbv in both sets of simulations. During the second half of the century, both models show an expansion of the heavily polluted area at Northern Hemisphere middle latitudes to cover virtually all longitudes except for the central Pacific. Increases during this period are in the range of 25–30 ppbv over the most polluted regions, with values greater than about 10 ppbv extending all the way to the Arctic in both models. The OsloCTM-1 results are also similar. Though they focus on changes in July, and thus find generally larger magnitudes in comparison to the annual average values reported by the other models, the spatial patterns are in good agreement both near the surface and in the upper troposphere.

[13] Using the same criteria for tropospheric air as in the column calculation, namely ozone values less than 150 ppbv (which leaves out 15–20% of the ozone below 150 hPa), we find an increase in the tropospheric ozone burden from 256 Tg in 1890 to 355 Tg in 1990. Using instead all ozone below 150 hPa, our burden increases from 297 to 425 Tg (Figure 2). This 39–43% increase is somewhat larger than the 71 Tg (~30%) increases seen in the MOZART-2 study. There are several possible explanations for this difference. The two models have a large difference in their tropospheric ozone burden, which is only 274 Tg for MOZART-2 in 1990. This is at least in part due to the difference between our upper boundaries and the 200 hPa boundary used for budget calculations in the other study. The two models also have different representations of the complex chemistry of hydrocarbons, and perhaps most importantly, different natural emissions. Since ozone responds nonlinearly to NO_x changes, having a different background state can greatly affect the results. Since the sensitivity does not change greatly going from a 150 hPa to a 150 ppbv ozone upper boundary in our model, we expect that the differences between the models stem more from the different background composition states. As noted by *Lamarque et al.* [2005], the preindustrial to present-day tropospheric ozone burden increase in MOZART-2 is at the low end of that seen in other models. Since both models reproduce present-day observations reasonably well, it is not clear which present-day burden or which sensitivity is more realistic. However, the sensitivity of the climate forcing is less than that of the burden, with variations up to 26% of the mean amongst models in the burden, but only 17% in the forcing [*Ramaswamy et al.*, 2001]. This suggests that the ozone response in the low-latitude middle and upper

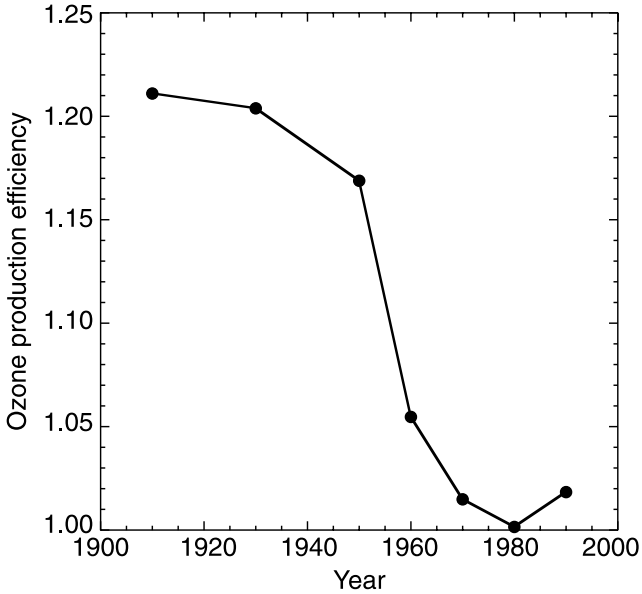

Figure 4. Normalized ozone production efficiency as a function of time. The efficiency is defined as the ratio of the increase in tropospheric ozone burden to the increase in NO_x emissions, both relative to 1890. The tropospheric burden was calculated using the 150 ppbv ozone threshold for stratospheric air, and the unitless efficiency was normalized for clarity (the 1980 value was 4.4). Dots indicate years when simulations were performed.

troposphere, which has the largest effect on radiative forcing, may be more consistent in the models than the response in other regions. Nevertheless, the uncertainty in the forcing remains sizable.

[14] The production efficiency of ozone from NO_x, defined as the ratio of the increase in the tropospheric ozone burden to the increase in NO_x emissions, both relative to 1890, was about 20% larger through 1950, decreasing thereafter, but remaining roughly constant since 1970 (Figure 4). These temporal changes are similar to the MOZART-2 study except that the steep reduction in efficiency began ~20 years earlier in their simulations. The fractional changes were greater in their study however, where the efficiency was reduced by roughly 33% (though they calculated the ozone burden change only below 400 hPa in this case, which limits the comparison and also limits comparison of the magnitude of the production efficiency in the two models). Again the discrepancies are most likely related to differing natural emissions and upper boundary specifications. In another study that used an entirely different chemistry transport model, the present-day efficiency of ozone production from NO_x emissions was found to be ~50% of the preindustrial value [*Wang and Jacob*, 1998]. Though that calculation covered a slightly longer time interval, it appears from the three studies that the magnitude of the efficiency change is not a robust quantity. In general, though, the timing and spatial patterns throughout the troposphere are broadly consistent between the MOZART-2, OsloCTM-1, and GISS models, though the magnitude of the ozone changes and the resulting forcing show sizable model-to-model variations.

4. Climate Response

[15] To evaluate the impact of the modeled tropospheric ozone changes with time on climate, we use the 3D ozone fields in transient coupled model simulations. The climate model's radiation code uses the ozone fields for online calculations of radiative transfer. It linearly interpolates between the monthly mean values for the 1890, 1910, 1930, 1950, 1960, 1970, 1980, and 1990 time slices, and then linearly interpolates again between monthly values to find the ozone for any particular day. Tropospheric ozone is not changed after 1990. Ozone values from the chemistry model are prescribed up to 150 hPa in the tropics, lowering from 150 to 200 hPa from 45 to 60° latitude, and to 290 hPa poleward of 60°. Above these levels, a present-day satellite climatology was used. A tropospheric decrease associated with polar springtime stratospheric ozone losses was also included (on the basis of observations [*Oltmans et al.*, 1997]), so that the model used the same tropospheric ozone change that is used in GISS simulations for the Intergovernmental Panel on Climate Change (IPCC) Fourth Assessment Report (AR4) along with other time-dependent forcings (J. Hansen et al., Climate simulations for 1880–2100 with GISS modelE, submitted to *Journal of Geophysical Research*, 2006, hereinafter referred to as Hansen et al., submitted manuscript, 2006). However, as the tropospheric decrease was small, seasonal, and only occurred during the last two decades of the 20th century (and only then at high latitudes, primarily over Antarctica, where there is little radiation in any case), this should have minimal influence on our results. To allow comparison with the IPCC AR4 simulations, the transient tropospheric ozone-only runs were performed with the same model version, namely the GISS Model III/ModelE coupled ocean-atmosphere model with 20 vertical layers and 4 by 5 degree horizontal resolution as detailed by *Schmidt et al.* [2006] using the ocean model of *Russell et al.* [1995]. An ensemble of five runs, extending from 1880 to 2003 and differing only in their initial conditions, was performed.

[16] For relatively short-lived trace species such as ozone, transport timescales separate the troposphere into three regions: the tropics and the two extratropical areas [*Bowman and Erukhimova*, 2004]. The ensemble mean global, tropical (24 S–24 N), NH and Southern Hemisphere (SH) extratropical annual average surface temperature trends in response to tropospheric ozone increases are shown in Figure 5. While a sizable amount of multidecadal variability is present from the ocean, especially in a seesaw in heat transport between the two extratropical regions, it is nevertheless quite clear that the climate response was spatially very inhomogeneous. The SH extratropics exhibited virtually no trend, the tropics warm substantially, and the NH extratropics warm quite rapidly. The linear trends over the 20th century are 0.03°C ± 0.01°C, 0.14°C ± 0.01°C, and 0.18°C ± 0.01°C, respectively (2 sigma uncertainty). The greater warming in the NH extratropics is consistent with the spatial distribution of ozone changes shown in Figure 3.

[17] Given the quasi-linearity in the ozone forcing during the first and second halves of the 20th century, it is

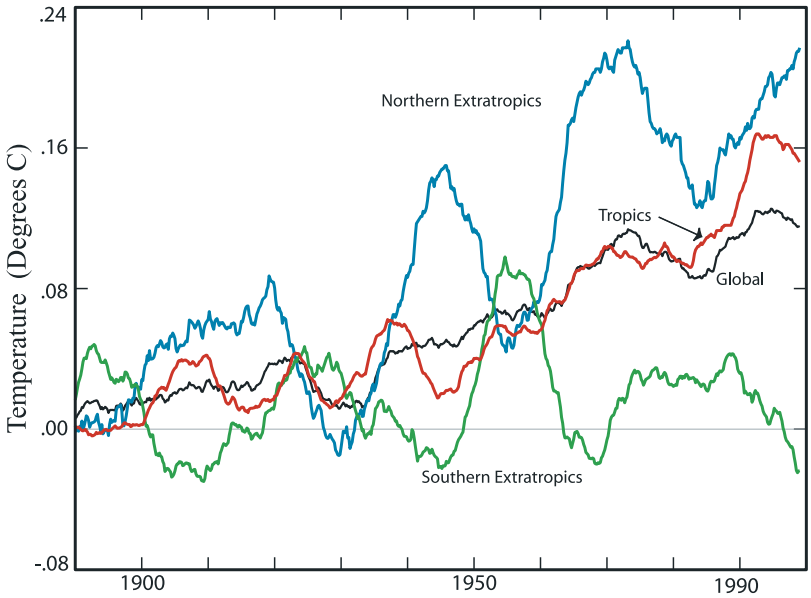

Figure 5. Annual average surface temperature variation in response to time-dependent tropospheric ozone change. Results are averages over the five ensemble members for the northern and southern extratropics, the tropics, and the entire globe, all smoothed with a 10-year running mean. Values are given relative to the 1880–1890 ensemble mean.

interesting to examine the climate response during these two periods. Since there is a lag time for the climate system to respond to forcing, especially via the ocean, it should not affect the results greatly that the forcing is unchanged after 1990. The linear trends during the two 50-year periods are shown in Figure 6. For comparison, we also show results from transient ensembles with the same model driven by changes in greenhouse gases, tropospheric aerosols (sulfate, black carbon, organic carbon, and nitrate), and all forcings (the above plus stratospheric ozone, solar variations, volcanic eruptions, a parameterization of the aerosol indirect effect, and the effect of soot on snow/ice albedo (see Hansen et al., submitted manuscript, 2006)). Fifty-year linear trends obtained from the GISS Surface Air Temperature Analysis (GISTEMP) observations are also shown [*Hansen et al.*, 2001]. The observations show greater warming in the NH extratropics than in other areas, consistent with the response to tropospheric ozone. However, the response to greenhouse gases exhibits similar behavior, and the net result is also quite sensitive to tropospheric aerosols, which will offset much of the asymmetry between regions by inducing greater cooling in the NH extratropics.

[18] The time dependence of the trends provides an additional way to identify the response to tropospheric ozone increases. While the extratropics in both hemispheres show either statistically indistinguishable observed rates of change in the two 50-year periods or a slowdown in the warming rate, the tropics show an accelerated warming by 0.13°C during the latter half of the century. The climate response to tropospheric ozone increases also produces minimal (or no) increase in warming rates in the extratropics during the two times, but an accelerated warming by 0.08°C in the tropics during the latter half of the century. This appears to be due to emissions from the developing world increasing sharply, especially in Asia and in Africa (Figure 1). Given the greater available sunlight at these latitudes compared with northern industrialized regions, photochemical production of ozone from NO_x is more efficient [*Fuglestvedt et al.*, 1999], leading to the large tropical ozone increases during the latter half of the century shown in Figure 3. Though both greenhouse gases and tropospheric aerosols also have contributed to the different rates of tropical temperature change in the two time periods, both of those led to substantial differences between the two 50-year periods in both extratropical regions as well, which was not seen in observations. While a fortuitous cancellation of opposing greenhouse warming and aerosol cooling is a possibility, tropospheric ozone increases seem very likely to have contributed to the more rapid warming of the tropics in the latter half of the 20th century.

[19] We can also examine the full spatial pattern of the climate response to tropospheric ozone increases. Given the greater noise when no spatial averaging is used, the most robust results are obtained from the ensemble mean linear trends over the full 20th century (Figure 7), though as noted previously the rates of temperature change, especially in the tropics, have not been uniform. The trends are quite inhomogeneous, with the largest warming over northern continental areas and in the Arctic. Though the radiative forcing follows the pattern of ozone column change extremely closely, as in other studies [*Kiehl et al.*, 1999], the climate response does not conform closely to the forcing. While the warming over the oceans does peak in the locations of greatest radiative forcing, warming over land areas and sea ice areas is not collocated with forcing maxima.

[20] Ozone's lifetime decreases during the summer in the extratropics as photochemical destruction rates increase

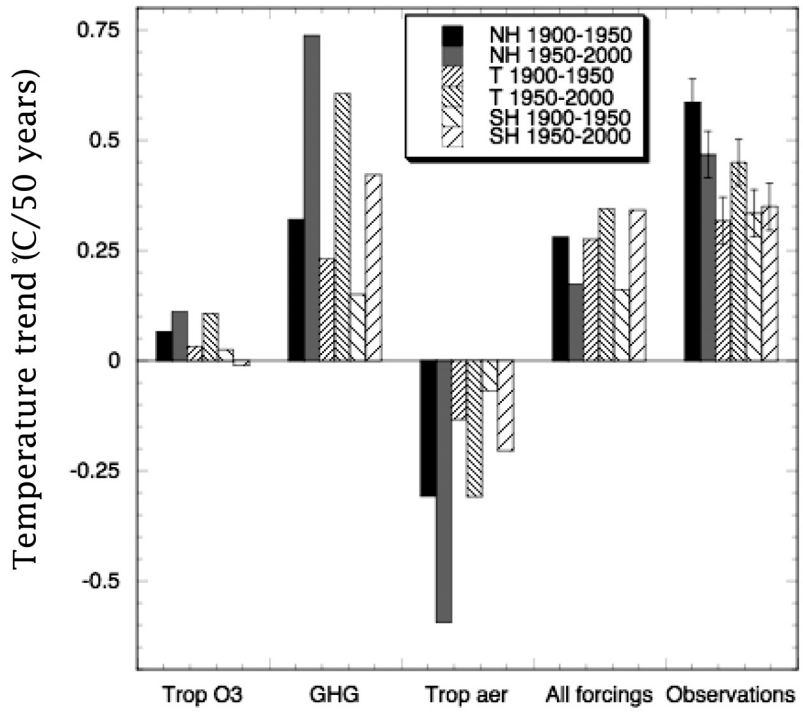

Figure 6. Half-century trends (°C per 50 years) for the northern extratropics, the tropics, and the southern extratropics in the GCM in response to the indicated forcings and in observations from GISTEMP [*Hansen et al.*, 2001]. The tropics is defined here as 24°S–24°N. The error bars on the observations indicate the 95% confidence level (two standard deviations) from the linear regression. All data are analyzed using a 30-year running mean to calculate annual trends (to remove the decadal variability apparent in Figure 5), which are then mapped onto the entire 50-year period. Model results are from five-member ensembles and thus have two standard deviation values of less than 0.05°C and typically less than 0.02°C. Note that the sums of the 50-year linear trends will not necessarily match the total change over the full century.

with greater insolation. Thus summer ozone has the largest radiative impact relatively near the precursor emission regions, leading to the maxima in summer warming occurring over polluted NH continental areas (Figure 7). The warming is especially pronounced over western North America and Eastern Europe/Central Asia, a pattern that persists into the annual average. Interestingly, observed linear trends in surface temperature over this same period also show enhanced warming over these two areas.

[21] The cold season is a time of relatively low ozone values over most areas, and reduced radiative forcing. However, as both an infrared-absorbing greenhouse gas and a shortwave absorber, ozone can induce especially large warming over highly reflective surfaces (where ozone has two chances to catch shortwave photons). This feature is clearly seen in the very large warming in snow and ice covered northern latitudes during boreal winter and over deserts. In the Arctic, however, there is so little radiation that direct ozone forcing alone cannot account for the large simulated winter warming (Figure 7). Zonal mean trends in the Arctic from the various model runs and observations are given in Table 1. As with the temporal trends, the results are dominated by the larger, partially offsetting, greenhouse gas-induced warming and tropospheric aerosol-induced cooling. The observations show enhanced warming over the Arctic during boreal winter, again consistent with the spatial structure of the modeled response to tropospheric ozone trends. The relative importance of tropospheric ozone is substantial in the Arctic during winter and spring, when it is roughly 25% as effective as greenhouse gases (Table 1). In comparison with its large role in the Arctic during fall, winter and spring, the contribution of tropospheric ozone to the global annual warming trend is less than 10% of that due to greenhouse gases. Ozone appears to induce similar polar amplification to that seen in response to other forcings (via sea ice, for example). The seasonal variation in the response to ozone is larger than in the response to other forcings, however (Table 1). This results mainly from ozone's shortened lifetime during the summer, which means that ozone is not effectively transported to the Arctic from polluted lower latitudes. The contribution of tropospheric ozone increases to the observed Arctic warming trends may have been substantial, as the response is roughly 30% of the measured trend during winter and roughly half the value of the net trend during fall and spring. The simulation with all forcings produces significantly more warming than observed in this region during fall, but the model's sensitivity appears to match the observations well during other seasons. However, variability is quite large in the Arctic, so that both the observed trends and the modeled climate response to ozone

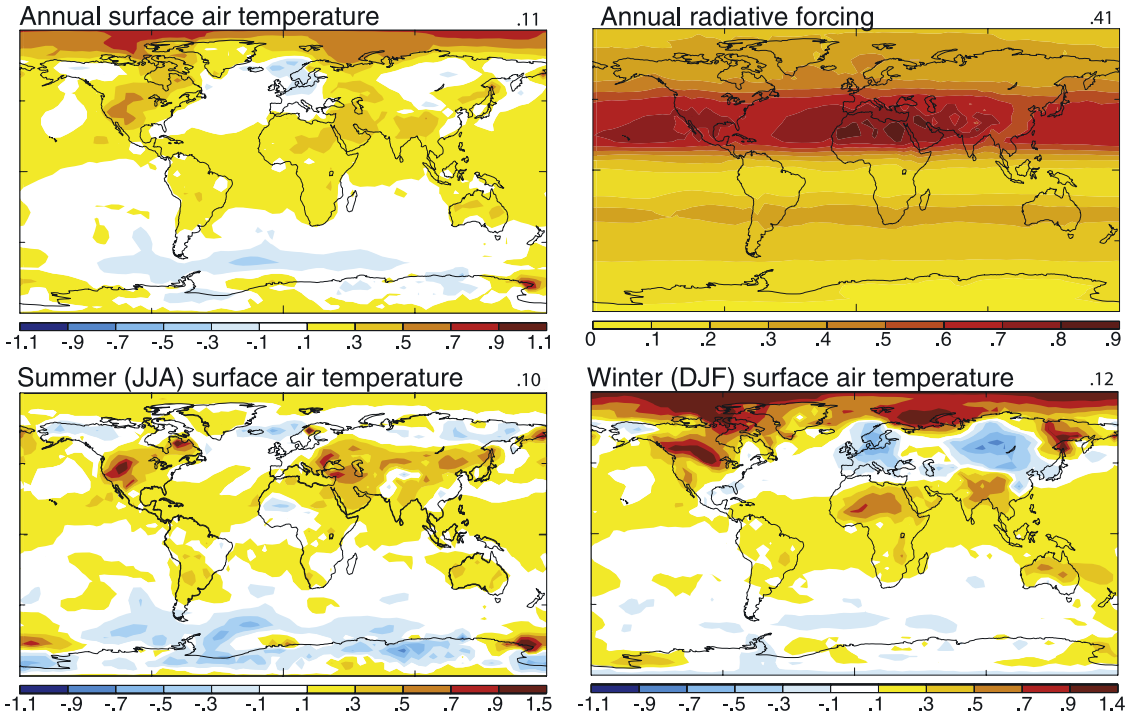

Figure 7. Ensemble average 1900–2000 surface temperature trends (°C per century) in response to tropospheric ozone changes and the input radiative forcing (W m^{-2}). Values are surface temperature trends for (top left) the annual average, (bottom left) June–August, and (bottom right) December–February and (top right) annual average tropopause instantaneous radiative forcing from 1880 to 1990. Temperature trends greater than about 0.1°C are significant over the oceans, while values greater than 0.3°C are typically significant over land, except for northern middle and high latitudes during winter where values in excess of about 0.5°C are significant. Values in the top right corner give area-weighted global averages in the same units as the plots.

are significant only during winter. Thus definitive analysis of Arctic temperature trends will require longer data sets. However, given the large amounts of ozone precursors produced at NH midlatitudes and the long lifetime of ozone transported poleward outside the summer season, it is reasonable that ozone would have a proportionally greater influence on the Arctic relative to the global average than would well-mixed gases. Outside the Arctic, in darker regions away from snow and ice cover, the warming during winter is typically quite small in extratropical regions.

5. Conclusions

[22] It is clearly more realistic to simulate the temporal and spatial distribution of tropospheric ozone changes than to assume a linear or exponential increase since the preindustrial. The use of tropospheric ozone with realistic temporal and spatial time dependence as a forcing should lead to more realistic climate simulations as well. However, the spatial and temporal response of Earth's surface temperatures during the 20th century was dominated by the larger forcings from greenhouse gases and tropospheric aerosols. Uncertainties in the latter, including the indirect effect of aerosols, make attribution of any observed climate change to a particular forcing such as tropospheric ozone challenging. Nevertheless, we've shown that several features of the response to tropospheric ozone increases are indeed in accord with observations. Specifically, our results suggest that tropospheric ozone trends may have contributed to the overall spatial pattern of 20th-century warming, especially at high latitudes during winter and spring and over polluted areas during summer. They also indicate that recent

Table 1. Zonal Mean Linear Trends in Surface Temperature (°C Per Century) over 1900–2000 Between Latitudes 70°–90°N[a]

	Winter	Spring	Summer	Fall
Greenhouse gases	2.19	1.81	0.48	2.10
Tropospheric ozone	0.52	0.43	0.04	0.20
Tropospheric aerosols	−0.68	−0.80	−0.62	−0.95
All forcings	1.44	1.38	0.20	1.01
Observations	1.76 ± 1.65	1.00 ± 1.17	0.29 ± 0.49	0.36 ± 1.11

[a]Observations are from the GISTEMP data set [*Hansen et al.*, 2001], model simulations as described in the text. The standard deviation of the model values is ~0.2°C during summer and ~0.4°C–0.5°C in other seasons (consistent with a five member ensemble with variability similar to that in the observations).

increases in economic development at low latitudes have led to rapid tropospheric ozone increases there during the latter half of the 20th century, which may have contributed to the accelerated warming seen in the tropics over that same period.

[23] The more widespread use of time-dependent tropospheric ozone changes in the next IPCC assessment may lead to improved simulations of the temporal and spatial patterns of climate change. Projections of future ozone precursor emissions show distinct differences from historical patterns, with greater development and hence emissions at low latitudes and improved pollution control strategies leading to decreases in emissions [*Dentener et al.*, 2004]. Thus the use of linear or exponential change with time is likely to become a much worse estimate than it is at present.

[24] Estimates of past forcing from tropospheric ozone increases remain subject to many uncertainties. Several factors may have biased our results toward small changes. Our model domain limit of 150 hPa did not include the uppermost tropical troposphere, which appears to reduce the magnitude of ozone forcing by ~20%. The source inventory used here had present-day biomass burning emissions that were significantly lower than other estimates, leading to temporal changes that were also low. Thus the forcing trend could be substantially larger than that simulated here, consistent with exploratory studies [*Mickley et al.*, 2001; *Shindell and Faluvegi*, 2002]. Interestingly, a greater role for tropospheric ozone in driving 20th-century climate change would improve agreement between the model and the observations (Figure 6).

[25] Since tropospheric ozone causes significant adverse human health impacts and also damages both natural and managed ecosystems, there are many benefits to be gained from reducing ozone pollution levels. Future trends are uncertain, however. This study helps characterize the climate effects of tropospheric ozone changes, enabling greater understanding of both the past effects of ozone increases and of the potential effects of future changes that could either increase or mitigate the rate of warming from long-lived greenhouse gases.

[26] **Acknowledgment.** This work was supported by NASA's Atmospheric Chemistry Modeling and Analysis Program.

References

Baughcum, S. L., T. G. Tritz, S. C. Henderson, and D. C. Pickett (1996), Scheduled civil aircraft emission inventories for 1992: Database development and analysis, *NASA Conf. Publ.*, *NASA CR-4700*.

Benkovitz, C. M., M. T. Scholtz, J. Pacyna, L. Tarrason, J. Dignon, E. C. Voldner, P. A. Spiro, J. A. Logan, and T. E. Graedel (1996), Global gridded inventories of anthropogenic emissions of sulfur and nitrogen, *J. Geophys. Res.*, *101*, 29,239–29,253.

Berntsen, T. K., I. S. Isaksen, G. Myhre, J. S. Fuglestvedt, R. Stordal, T. A. Larsen, R. S. Freckleton, and K. P. Shine (1997), Effects of anthropogenic emissions on tropospheric ozone and its radiative forcing, *J. Geophys. Res.*, *102*, 28,101–28,126.

Berntsen, T. K., G. Myhre, F. Stordal, and I. S. Isaksen (2000), Time evolution of tropospheric ozone and its radiative forcing, *J. Geophys. Res.*, *105*, 8915–8930.

Bowman, K. P., and T. Erukhimova (2004), Comparison of global-scale Langrangian transport properties of the NCEP reanalysis and CCM3, *J. Clim.*, *17*, 1135–1146.

Dai, A., T. M. A. Wigley, B. A. Boville, J. T. Kiehl, and L. E. Buja (2001), Climates of the twentieth and twenty-first centuries simulated by the NCAR climate system model, *J. Clim.*, *14*, 485–519.

Dentener, F., D. Stevenson, J. Cofala, R. Mechler, M. Amann, P. Bergamaschi, F. Raes, and R. G. Derwent (2004), The impact of air pollutant and methane emission controls on tropospheric ozone and radiative forcing: CTM calculations for the period 1990–2030, *Atmos. Chem. Phys. Disc.*, *4*, 8471–8538.

Fuglestvedt, J. S., T. K. Berntsen, I. S. A. Isaksen, H. Mao, X.-Z. Liang, and W.-C. Wang (1999), Climatic forcing of nitrogen oxides through changes in tropospheric ozone and methane: Global 3D model studies, *Atmos. Environ.*, *33*, 961–977.

Grenfell, J. L., D. T. Shindell, D. Koch, and D. Rind (2001), Chemistry-climate interactions in the Goddard Institute for Space Studies general circulation model: 2. New insights into modeling the preindustrial atmosphere, *J. Geophys. Res.*, *106*, 33,435–33,452.

Hansen, J. E., M. Sato, and R. Reudy (1997), Radiative forcing and climate response, *J. Geophys. Res.*, *102*, 6831–6864.

Hansen, J., R. Ruedy, M. Sato, M. Imhoff, W. Lawrence, D. Easterling, T. Peterson, and T. Karl (2001), A closer look at United States and global surface temperature change, *J. Geophys. Res.*, *106*, 23,947–23,963.

Hansen, J., et al. (2002), Climate forcings in Goddard Institute for Space Studies SI2000 simulations, *J. Geophys. Res.*, *107*(D18), 4347, doi:10.1029/2001JD001143.

Hauglustaine, D. A., and G. Brasseur (2001), Evolution of tropospheric ozone under anthropogenic activities and associated radiative forcing of climate, *J. Geophys. Res.*, *106*, 32,337–32,360.

Kiehl, J. T., T. L. Schneider, R. W. Portmann, and S. Solomon (1999), Climate forcing due to tropospheric and stratospheric ozone, *J. Geophys. Res.*, *104*, 31,239–31,254.

Lamarque, J.-F., P. Hess, L. Emmons, L. Buja, W. M. Washington, and C. Granier (2005), Tropospheric ozone evolution between 1890 and 1990, *J. Geophys. Res.*, *110*, D08304, doi:10.1029/2004JD005537.

Levy, H. I., P. S. Kasibhatla, W. J. Moxim, A. A. Klonecki, A. I. Hirsch, S. J. Oltmans, and W. L. Chameides (1997), The global impact of human activity on tropospheric ozone, *Geophys. Res. Lett.*, *24*, 791–794.

Meehl, G. A., W. M. Washington, C. M. Ammann, J. M. Arblaster, T. M. L. Wigley, and C. Tebaldi (2004), Combinations of natural and anthropogenic forcings in twentieth-century climate, *J. Clim.*, *17*, 3721–3727.

Mickley, L. J., P. P. Murti, D. J. Jacob, J. A. Logan, D. M. Koch, and D. Rind (1999), Radiative forcing from tropospheric ozone calculated with a unified chemistry climate model, *J. Geophys. Res.*, *104*, 30,153–30,172.

Mickley, L. J., D. J. Jacob, and D. Rind (2001), Uncertainty in preindustrial abundance of tropospheric ozone: Implications for radiative forcing calculations, *J. Geophys. Res.*, *106*, 3389–3399.

Oltmans, S. J., et al. (1997), Trends of ozone in the troposphere, *Geophys. Res. Lett.*, *25*, 139–142.

Pavelin, E. G., C. E. Johnson, S. Rughooputh, and R. Toumi (1999), Evaluation of preindustrial surface ozone measurements made using the Schönbein method, *Atmos. Environ.*, *33*, 919–929.

Ramaswamy, V., et al. (2001), Radiative forcing of climate change, in *Climate Change 2001*, edited by J. T. Houghton et al., pp. 349–416, Cambridge Univ. Press, New York.

Roeckner, E., L. Bengtsson, J. Feichter, J. Lelieveld, and H. Rodhe (1999), Transient climate change simulations with a coupled atmosphere-ocean GCM including the tropospheric sulfur cycle, *J. Clim.*, *12*, 3004–3032.

Roelofs, G.-J., J. Lelieveld, and R. Van Dorland (1997), A three-dimensional chemistry/general circulation model simulation of anthropogenically derived ozone in the troposphere and its radiative forcing, *J. Geophys. Res.*, *102*, 23,389–23,401.

Russell, G. L., J. R. Miller, and D. Rind (1995), A coupled atmosphere-ocean model for transient climate change, *Atmos. Ocean*, *33*, 683–730.

Schmidt, G. A., et al. (2006), Present day atmospheric simulations using GISS ModelE: Comparison to in-situ, satellite and reanalysis data, *J. Clim.*, *19*, 153–192.

Shindell, D. T., and G. Faluvegi (2002), An exploration of ozone changes and their radiative forcing prior to the chlorofluorocarbon era, *Atmos. Chem. Phys.*, *2*, 363–374.

Shindell, D. T., G. Faluvegi, and N. Bell (2003), Preindustrial-to-present-day radiative forcing by tropospheric ozone from improved simulations with the GISS chemistry-climate GCM, *Atmos. Chem. Phys.*, *3*, 1675–1702.

Shindell, D. T., G. Faluvegi, N. Bell, and G. A. Schmidt (2005a), An emissions-based view of climate forcing by methane and tropospheric ozone, *Geophys. Res. Lett.*, *32*, L04803, doi:10.1029/2004GL021900.

Shindell, D. T., G. Faluvegi, and L. K. Emmons (2005b), Inferring carbon monoxide pollution changes from space-based observations, *J. Geophys. Res.*, *110*, D23303, doi:10.1029/2005JD006132.

Staehelin, J., J. Thudium, R. Buehler, A. Volz-Thomas, and W. Graber (1994), Trends in surface ozone at Arosa (Switzerland), *Atmos. Environ.*, *28*, 75–87.

Stevenson, D. S., C. E. Johnson, W. J. Collins, R. G. Derwent, K. P. Shine, and J. M. Edwards (1998), Evolution of tropospheric radiative forcing, *Geophys. Res. Lett.*, *25*, 3819–3822.

United States Environmental Protection Agency (2000), National air pollutant emissions trends, 1900–1998, *EPA-454/R-00-002*, Research Triangle Park, N. C.

van Aardenne, J., F. Dentener, J. Olivier, C. K. Goldewijk, and J. Lelieveld (2001), A $1° \times 1°$ resolution data set of historical anthropogenic trace gas emissions for the period 1890–1990, *Global Biogeochem. Cycles*, *15*, 909–928.

Van der Werf, G. R., J. T. Randerson, G. J. Collatz, and L. Giglio (2003), Carbon emissions from fires in tropical and subtropical ecosystems, *Global Change Biol.*, *9*, 547–562.

Volz, A., and D. Kley (1988), Evaluation of the Montsouris series of ozone measurements made in the nineteenth century, *Nature*, *332*, 240–242.

Wang, Y. H., and D. Jacob (1998), Anthropogenic forcing on tropospheric ozone and OH since preindustrial times, *J. Geophys. Res.*, *103*, 31,123–31,135.

E. Aguilar, G. Faluvegi, J. Hansen, A. Lacis, and D. Shindell, NASA Goddard Institute for Space Studies, 2880 Broadway, New York, NY 10025, USA. (dshindell@giss.nasa.gov)

R. Ruedy, SGT Incorporated, 2880 Broadway, New York, NY 10025, USA.